Investigating conformation dependence and nonadiabatic effects in the photodissociation of allyl chloride at 193 nm

T. L. Myers, D. C. Kitchen, B. Hu, and L. J. Butler
The James Franck Institute and Department of Chemistry, The University of Chicago, Chicago, Illinois 60637

(Received 10 November 1995; accepted 4 January 1996)

The experiments presented here investigate the competing photodissociation pathways for allyl chloride upon excitation of the nominally $\pi\pi^*$(C═C) transition at 193 nm. The measured photofragment velocity distributions evidence C–Cl bond fission and HCl elimination. The recoil kinetic energy distribution for the HCl products is bimodal, indicating two primary processes for HCl elimination. The experimental measurements show C–Cl bond fission dominates, giving an absolute branching ratio of HCl:C–Cl=0.12±0.03 when the parent molecule is expanded through a nozzle at 200 °C. The branching ratio depends on the nozzle temperature; at 475 °C, the absolute branching ratio measured is HCl:C–Cl=0.24±0.03. We analyze the experimental results along with supporting *ab initio* calculations and earlier photodissociation studies of vinyl chloride in order to examine the potential influence of nonadiabaticity along the C–Cl fission reaction coordinate and its dependence on molecular conformation. © *1996 American Institute of Physics.*
[S0021-9606(96)01514-7]

I. INTRODUCTION

We chose to investigate the photodissociation pathways of allyl chloride at 193 nm in order to investigate a special class of organic reactions, those allowed by conservation of total electronic symmetry but Woodward–Hoffmann forbidden.[1] In both vinyl chloride and the *cis* conformer of allyl chloride, the potential energy surface reached with the $\pi\pi^*$ absorption has a barrier resulting from an avoided crossing between the $\pi\pi^*$(C═C) and the $n(\mathrm{Cl})\sigma^*$(C–Cl) configurations. Since the pathway to C–Cl fission on the excited state potential energy surface involves a change in individual orbital symmetry along the adiabatic reaction coordinate, C–Cl fission is Woodward–Hoffmann forbidden. Previous work in our group[2] has indicated that the reaction rates in Woodward–Hoffmann forbidden reactions are reduced due to nonadiabatic recrossing of the barrier. We have also shown[3] that increasing the distance between the orbitals involved in the avoided crossing decreases the electronic coupling and thus increases the probability of nonadiabatically recrossing the barrier. Thus the comparison between the photodissociation dynamics of allyl and vinyl chloride can test our understanding of this class of reactions.

Previous experiments[4,5] on the photodissociation of vinyl chloride at 193 nm have identified both C–Cl fission and HCl elimination as the primary reaction pathways. They proposed that the pathway to C–Cl fission is a predissociation from the photoprepared $\pi\pi^*_{\mathrm{C=C}}$ state to the repulsive $n_{\mathrm{Cl}}\sigma^*_{\mathrm{C-Cl}}$ state whereas the channel for HCl elimination is a ground state process following internal conversion.[5] The two processes compete with a branching ratio reported by Umemoto *et al.*,[5] C–Cl: HCl=1.1:1.0. Furthermore, Mo *et al.*[4] have observed two other minor primary reaction channels attributed to internal conversion, C–H bond fission and another pathway for C–Cl fission producing low energy Cl fragments.

The first band in the ultraviolet absorption spectrum of allyl chloride, a broad band peaking at 171 nm, is assigned to the $\pi\pi^*_{\mathrm{C=C}}$ transition.[6] Although no collisionless gas-phase photolysis experiments on allyl chloride in this absorption band have been published,[7] the photolysis of gaseous allyl chloride at 229 nm, which accesses the rising edge of the $\pi\pi^*_{\mathrm{C=C}}$ absorption band, has been studied by Sears and Volman.[8] They used chromatographic analysis to identify the products resulting from secondary reactions of the photodissociated products and concluded that the only primary dissociation process is C–Cl fission.

This work measures the photofragment velocities and angular distributions of allyl chloride at 193 nm with a crossed laser-molecular beam apparatus and determines the absolute branching ratios between HCl elimination and C–Cl fission at two nozzle temperatures. These results are compared to a similar system with no CH_2 spacer between the C–Cl and C═C chromophores, vinyl chloride. Analysis of our results allows us to investigate whether the excited state C–Cl reaction coordinate is traversed adiabatically or not in allyl chloride as compared to vinyl chloride by considering the A' adiabatic Born Oppenheimer potential energy surface formed from the avoided crossing of the $\pi\pi^*_{\mathrm{C=C}}$ and the $n_{\mathrm{Cl}}\sigma^*_{\mathrm{C-Cl}}$ states. Preliminary *ab initio* electronic structure calculations of the potential energy surfaces are also presented to help interpret the experimental results by providing the energetic splittings between the adiabatic excited electronic states at the avoided crossing in the C–Cl bond fission channel.

II. EXPERIMENT

A. Molecular beam experiments

The experiments here measure the velocity and angular distributions of the photofragments from the photodissociation of allyl chloride, CH_2═$CHCH_2Cl$, at 193 nm using a

 0021-9606/96/104(14)/5446/11/$10.00

crossed laser-molecular beam apparatus. After excitation with a pulsed excimer laser, the fragments photodissociate from the crossing point of the laser and molecular beam with velocities determined by the vector sum of the molecular beam velocity and the recoil velocity imparted in the dissociation. The fragments that scatter into the differentially pumped detector travel 44.1 cm to an electron bombardment ionizer where they are ionized by 200 eV electrons. The ions are mass selected with a quadrupole mass filter and counted with a Daly detector and multichannel scalar with respect to their time of flight (TOF) from the interaction region after the dissociating laser pulse.

The molecular beam was formed by bubbling He carrier gas through the liquid allyl chloride, cooled to -25 °C to maintain a vapor pressure of roughly 20 Torr, to give a total stagnation pressure of 300 Torr. The 0.076 mm diam nozzle was heated to 220 °C in order to prevent cluster formation during the supersonic expansion. For the branching ratio data, we used nozzle temperatures of 200 °C and 475 °C. The velocity of the parent molecular beam was measured by rotating the molecular beam source to point into the detector and raising a chopper wheel into the beam.

A Lumonics PM-848 excimer laser with an ArF fill was used to produce the photolytic wavelength. The unpolarized laser power was typically 25 mJ/pulse and focused to a 5 mm^2 spot size in the interaction region.

The source angle was maintained at 15° with respect to the detector axis. The strong signal observed at $m/e^+=35$, Cl^+, after 300 000 shots corresponds to predominantly C–Cl fission but also has a significant contribution from the Cl^+ daughter ion of HCl photofragments. The momentum-matched fragment for the Cl atom, CH_2CHCH_2, was detected at the parent ion, $m/e^+=41$, after 1 500 000 laser shots. The signal observed at $m/e^+=36$ after 1 000 000 shots was attributed to HCl elimination. The momentum-matched partner for HCl, C_3H_4, was observed at the parent ion, $m/e^+=40$, after 2 500 000 shots, but the signal also has a contribution from a daughter ion of the momentum-matched fragment of the Cl atom. Signal was also observed at $m/e^+=39$, 38 and 37 and, although not shown, were adequately fit with contributions from the above dissociation channels. No signal was seen at $m/e^+=49$, CH_2Cl^+, after 500 000 shots.

B. Computational method

To help interpret the experimental results, we also present *ab initio* electronic structure calculations for vinyl chloride[9(a)] and *cis*- and *gauche*-allyl chloride[9(b)] using the GAUSSIAN 92 system of programs[10] with a 6-311G* basis set. Configuration interaction with single and double excitations (CISD) calculations provide electronic ground state energies in the harmonic region of the C–Cl stretching potentials. These energies are then fit to Morse potentials with the correct dissociation energies, 80 kcal/mol for vinyl chloride and 68 kcal/mol for allyl chloride.[11] Configuration interaction with single excitations (CIS) calculations provide excitation energies from the ground electronic state to the relevant excited electronic states. These CIS excitation energies are added to the ground-state Morse oscillator energies to construct the excited electronic state surfaces.

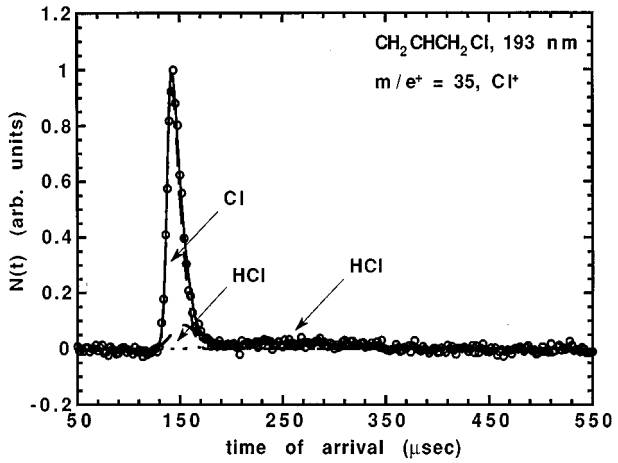

FIG. 1. The laboratory TOF spectrum of the photofragments detected at Cl^+ from allyl chloride photodissociated at 193 nm with a nozzle temperature of 220 °C and a source angle of 15°. The contribution from Cl fragments to the Cl^+ signal was determined by fitting the signal with the $P(E_T)$ for primary C–Cl fission in Fig. 3. Similarly, the contribution from HCl fragments was determined by fitting the signal with the $P(E_T)$'s for primary HCl elimination in Fig. 4.

III. RESULTS AND ANALYSIS

A. Identification of primary product channels

The data for allyl chloride excited at 193 nm evidence three competing channels, C–Cl bond fission and two different pathways for HCl elimination. Figure 1 shows the TOF spectrum taken at $m/e^+=35$, Cl^+, attributed to signal from primary C–Cl fission as well as HCl cracking in the ionizer to give Cl^+ as a daughter ion. The contribution from C–Cl fission is determined by forward convolution fitting of the TOF for the momentum-matched fragment, $CH_2CHCH_2^+$, in Fig. 2 to derive the center-of-mass product translational energy distribution, $P(E_T)$, for C–Cl fission. This $P(E_T)$ is then used to fit the TOF spectrum at $m/e^+=35$. The remaining signal in the Cl^+ spectrum is fit by the two pathways for HCl elimination. The relative scaling of the two contributions was retained from the $m/e^+=36$ data presented later. Figure 3 shows the $P(E_T)$ for C–Cl fission, which peaks at 45 kcal/mol and extends out to near 60 kcal/mol, two-thirds of the maximum 80 kcal/mol[11] of available energy. The translational energy distribution for C–Cl fission indicates there is a significant exit channel barrier along the reaction coordinate since it peaks well away from zero. Thus, the pathway to C–Cl fission must occur along an excited state surface since the barrier to the reverse reaction on the ground state surface is typically negligible. Although some Cl atoms with low translational energies were observed for vinyl chloride and attributed to an internal conversion mechanism,[4] no evidence for this pathway in allyl chloride is found.

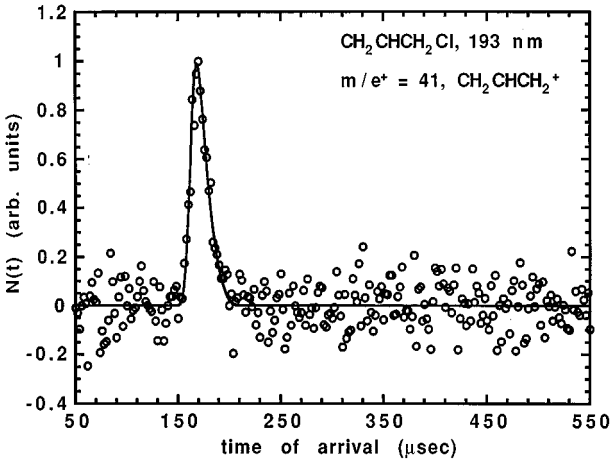

FIG. 2. The laboratory TOF spectrum of the photofragments detected at $CH_2CHCH_2^+$ from allyl chloride photodissociated at 193 nm with a nozzle temperature of 220 °C and a source angle of 15°. The signal is fit with the $P(E_T)$ in Fig. 3 showing the required momentum match between the Cl and the CH_2CHCH_2 fragments for primary C–Cl fission.

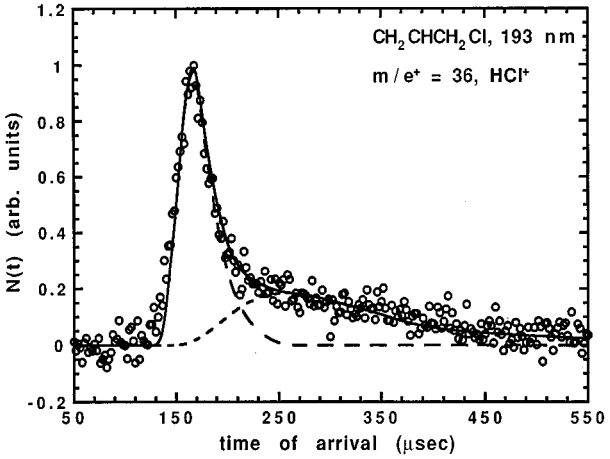

FIG. 4. The laboratory TOF spectrum of the photofragments detected at HCl^+ from allyl chloride photodissociated at 193 nm with a nozzle temperature of 220 °C. The source angle was 15°. The fastest portion of the signal is fit with the $P(E_T)$ shown in the top frame of Fig. 5, and the slowest portion of the signal is fit with the $P(E_T)$ shown in the bottom of Fig. 5, both corresponding to primary HCl elimination. The fast peak cannot be fit by assuming it results from the unlikely C_3^+ daughter ion of the CH_2CHCH_2 product of C–Cl fission.

As shown in the TOF spectrum for $m/e^+=36$, HCl^+, in Fig. 4, two different pathways for HCl elimination occur at 193 nm. One channel yields fragments with high translational energies; the fast component of the HCl^+ spectrum is fitted with the $P(E_T)$ shown in the top frame of Fig. 5. This $P(E_T)$, which peaks at 34 kcal/mol and extends out to 76 kcal/mol, evidences a large barrier to reverse reaction. The other channel produces low energy HCl fragments, and the $P(E_T)$ in the bottom frame of Fig. 5 fits the slow component in the HCl^+ spectrum. This $P(E_T)$ indicates smaller repulsive exit channel forces since it peaks at 3.6 kcal/mol. The two pathways could result from either HCl elimination occurring from different potential energy surfaces or from two different mechanisms on the same surface. In Sec. IV, we analyze the possible assignments for the two observed HCl elimination channels.

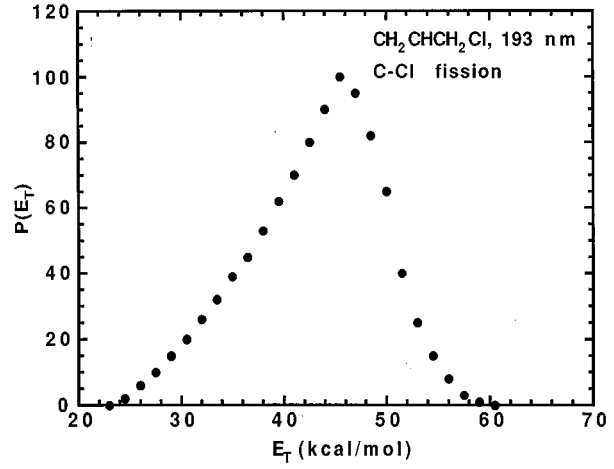

FIG. 3. The center-of-mass product translational energy distribution, $P(E_T)$, for the C–Cl fission channel in allyl chloride at 193 nm. The $P(E_T)$ is derived from forward convolution fitting the $CH_2CHCH_2^+$ signal in Fig. 2 which results from primary C–Cl fission.

Since studies[4] of the photodissociation channels of vinyl chloride at 193 nm have detected a slow kinetic energy C–Cl fission channel attributed to internal conversion, we took care to analyze whether our data might indicate this channel. We must assign the slow signal at Cl^+ in Fig. 1 between 160 and 400 μs to HCl elimination rather than a slow C–Cl channel for two reasons. First, the data is fit very well by assigning all of the slow signal to a daughter ion of HCl; it has the same velocity distribution as the slow signal at $m/e^+=36$ for HCl^+ shown in Fig. 4. Second, the slow HCl products in the $m/e^+=36$ data increase markedly with temperature, and the slow Cl^+ data shows the same increase. This can easily be seen by the similar cracking pattern of HCl calculated from the high vs the low temperature data (the cracking pattern of HCl, calculated from the ratio of the slow HCl^+ to slow Cl^+ signal in the next section, does not change with nozzle temperature). As a further check, since the secondary dissociation of very slow allyl radicals from C–Cl fission is possible (so one would not see evidence of a slow C–Cl fission channel at $m/e^+=41$), we present in Fig. 6 the $m/e^+=40$ signal which can be adequately fit with contributions from the assigned dissociation channels.

Two other possible primary photodissociation channels, C–H bond fission and H_2 elimination, are not investigated in these experiments since the momentum-matched fragments would be too heavy to recoil out to the detection angles sampled. Data at H_2^+ and H^+ was not taken due to the high background at these masses and the low ionization cross sections of H atom and H_2, which prohibit their efficient detection in our apparatus.

B. Product branching ratios

With careful analysis, the data allows the determination of the absolute branching ratio of the HCl elimination pro-

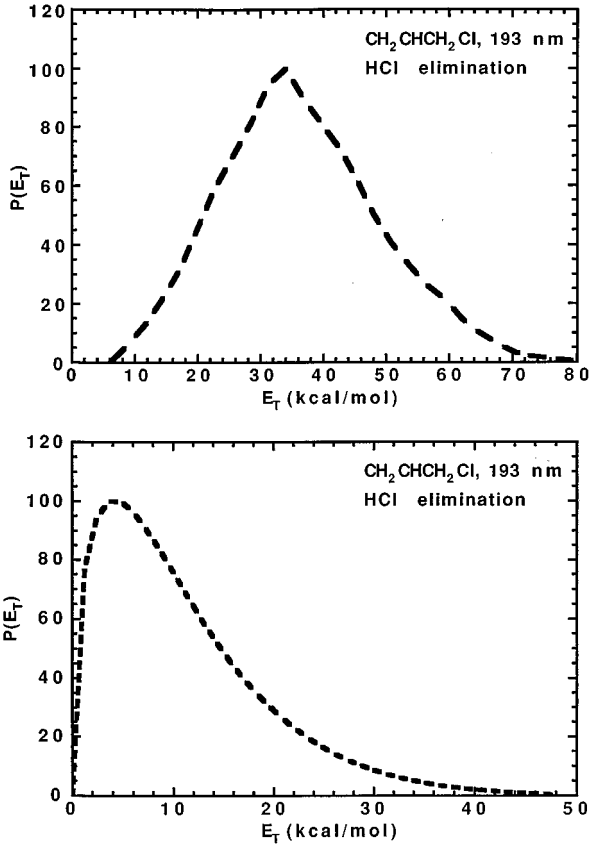

FIG. 5. The center-of-mass product translational energy distributions for the HCl elimination channels in allyl chloride at 193 nm. The $P(E_T)$ in the top frame is derived from forward convolution fitting the fastest portion of the HCl^+ signal in Fig. 4, and the $P(E_T)$ in the bottom frame is derived from forward convolution fitting the slowest portion of the HCl^+ signal in Fig. 4. The very high energy portion (>30 kcal/mol) of the low energy $P(E_T)$ cannot be uniquely determined because the signal overlaps strongly with the high energy channel at these energies.

cesses and the C–Cl bond fission pathway. To average out systematic errors, we integrated the TOF spectra at Cl^+ (Fig. 7) and HCl^+ (Fig. 8), taken with a nozzle temperature of 200 °C, for a total of 210 000 and 1 050 000 shots respectively, changing the mass from $m/e^+=35$ and $m/e^+=36$ every 30 000 and 150 000 shots respectively for a total of 7 scans each. The TOF spectra at Cl^+ (Fig. 9) and HCl^+ (Fig. 10) at 475 °C nozzle temperature, were also recorded for 50 000 and 100 000 shots respectively for a total of four scans each in order to determine if there was a temperature dependence. Using the measured kinetic energy distributions for C–Cl fission and HCl elimination in Figs. 3 and 5, we fit the Cl^+ and HCl^+ TOF data by adjusting the relative probabilities until a good fit is obtained. As previously noted, we retain the relative scaling between the two HCl elimination pathways used to fit the TOF spectra in Fig. 8 and Fig. 10 when we fit the corresponding Cl^+ spectra in Fig. 7 and Fig. 9. The absolute branching ratio between both pathways for HCl elimination and C–Cl fission can be calculated from the relative probabilities, which already incorporate corrections for kinematic factors, used to fit the Cl^+ spectrum at 200 °C by simply accounting for the daughter-ion fragmentation pattern of HCl. (The angular distributions of the HCl elimination pathways are assumed to be isotropic.) Assuming that the cracking pattern of the HCl fragment is identical for the two pathways and does not change with nozzle temperature, we integrate the slow signal for HCl elimination at the higher temperature from 248–400 μs for both the HCl^+ and Cl^+ TOF spectra to determine the fragmentation pattern of HCl to HCl^+/Cl^+. After correcting the integrated signal for the

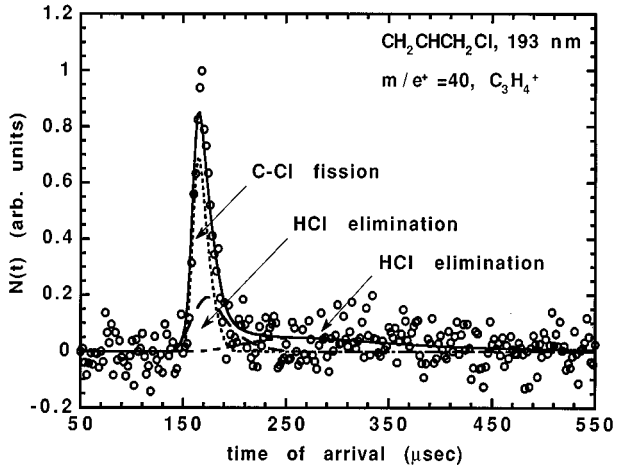

FIG. 6. The laboratory TOF spectrum of the photofragments detected at $C_3H_4^+$ from allyl chloride photodissociated at 193 nm with a nozzle temperature of 200 °C and a source angle of 15°. The signal is fit with the $P(E_T)$'s for primary HCl elimination in Fig. 4 showing the required momentum match between the HCl and the C_3H_4 fragments and with the daughter ion of the momentum-matched fragment for C–Cl fission.

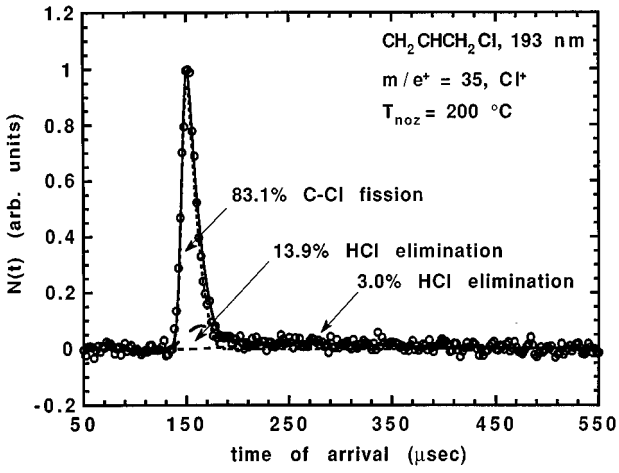

FIG. 7. The laboratory TOF spectrum of the photofragments detected at Cl^+ from allyl chloride photodissociated at 193 nm with a nozzle temperature of 200 °C and a source angle of 15°. The contribution from Cl fragments to the Cl^+ signal was determined by fitting the signal with the $P(E_T)$ for primary C–Cl fission in Fig. 3. Similarly, the contribution from HCl fragments was determined by fitting the signal with the $P(E_T)$'s for primary HCl elimination in Fig. 4 in which the relative scaling of the two pathways was retained from the HCl^+ TOF in Fig. 8. This data was used to determine the absolute branching ratios at 200 °C. The percent contributions from each channel shown are the relative probabilities that already include kinematic factors but do not yet account for ionization cross sections and cracking probabilities.

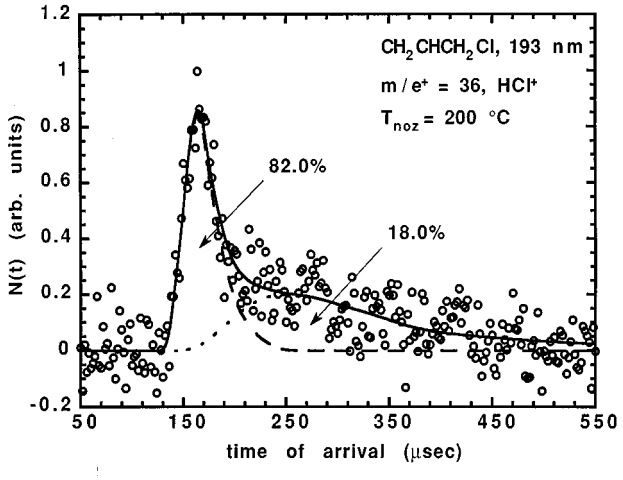

FIG. 8. The laboratory TOF spectrum of the photofragments detected at HCl^+ from allyl chloride photodissociated at 193 nm with a nozzle temperature of 200 °C and a source angle of 15°. The contribution from HCl fragments was determined by fitting the signal with the $P(E_T)$'s for primary HCl elimination in Fig. 4. The percent contributions from each channel shown are the relative probabilities that already include kinematic factors but do not yet account for ionization cross sections and cracking probabilities.

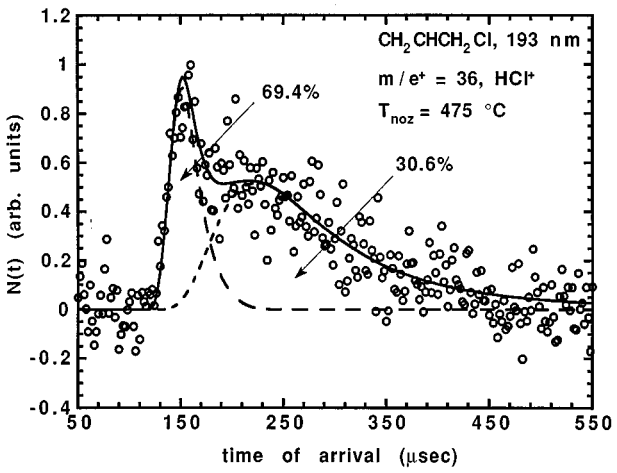

FIG. 10. The laboratory TOF spectrum of the photofragments detected at HCl^+ from allyl chloride photodissociated at 193 nm with a nozzle temperature of 475 °C and a source angle of 15°. The contribution from HCl fragments was determined by fitting the signal with the $P(E_T)$'s for primary HCl elimination in Fig. 4. The percent contributions from each channel shown are the relative probabilities that already include kinematic factors but do not yet account for ionization cross sections and cracking probabilities.

number of laser shots, we calculate the experimentally determined fragmentation pattern of HCl to HCl^+/Cl^+ to be 0.68 $\pm$0.08 (all error bars are reported as 2σ). We also calculate the fragmentation pattern of HCl from the data at 200 °C and obtain $HCl^+/Cl^+ = 0.71 \pm 0.19$ in order to verify that the ratio is the same at the two temperatures; however, we do not use this value in our branching ratio calculations. We then correct the branching ratio for the relative ionization cross sections of the Cl and HCl fragments, which are estimated from their polarizabilities to be $\sigma_{\text{ion}}^{\text{Cl}} = 2.18$ Å^3 and $\sigma_{\text{ion}}^{\text{HCl}} = 2.60$ Å^3 respectively.[12]

$$\left(\frac{\text{total HCl elimination}}{\text{C–Cl fission}}\right)_{200\,^\circ\text{C}} = \frac{(\%\text{HCl}_{\text{fast}} + \%\text{HCl}_{\text{slow}})}{\%\text{C–Cl}} \cdot \frac{\sigma_{\text{ion}}^{\text{Cl}}}{\sigma_{\text{ion}}^{\text{HCl}}} \cdot \frac{\text{HCl}^+}{\text{Cl}^+}. \quad (1)$$

The final result is a primary product branching ratio of $(\text{HCl:C–Cl})_{200\,^\circ\text{C}} = 0.12:1.0 \pm 0.03$. Similarly, we determined the branching ratio for the data with a nozzle temperature of 475 °C, obtaining a primary product branching ratio of $(\text{HCl:C–Cl})_{475\,^\circ\text{C}} = 0.23:1.0 \pm 0.03$. This result shows the branching ratio between HCl elimination and C–Cl fission increases when the nozzle temperature is raised.

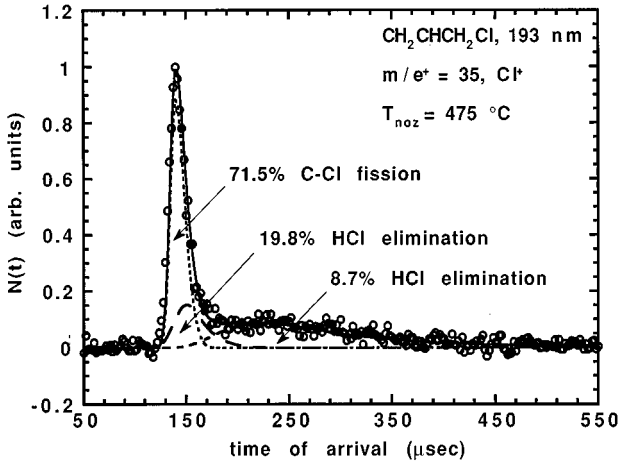

FIG. 9. The laboratory TOF spectrum of the photofragments detected at Cl^+ from allyl chloride photodissociated at 193 nm with a nozzle temperature of 475 °C and a source angle of 15°. The contribution from Cl fragments to the Cl^+ signal was determined by fitting the signal with the $P(E_T)$ for primary C–Cl fission in Fig. 3. Similarly, the contribution from HCl fragments was determined by fitting the signal with the $P(E_T)$'s for primary HCl elimination in Fig. 4 in which the relative scaling of the two pathways was retained from the HCl^+ TOF in Fig. 10. These data were used to determine the absolute branching ratios at 475 °C. The percent contributions from each channel shown are the relative probabilities that already include kinematic factors but do not yet account for ionization cross sections and cracking probabilities.

C. Analysis of the temperature dependence of the branching ratios with respect to conformer populations

As shown in the section above, the HCl elimination/C–Cl fission branching ratio depends strongly on the nozzle temperature. Since negligible conformer relaxation in the expansion occurs for allyl chloride,[13] the fraction of the higher energy *cis* conformer is increased upon raising the nozzle temperature. Thus, we now analyze the data to investigate whether the change in the branching ratio results from the change in the conformer populations. Although gas phase studies on the conformational properties of allyl chloride have been investigated,[14,15] a reliable energy difference has not been reported. Schei and Shen[14] used electron diffraction

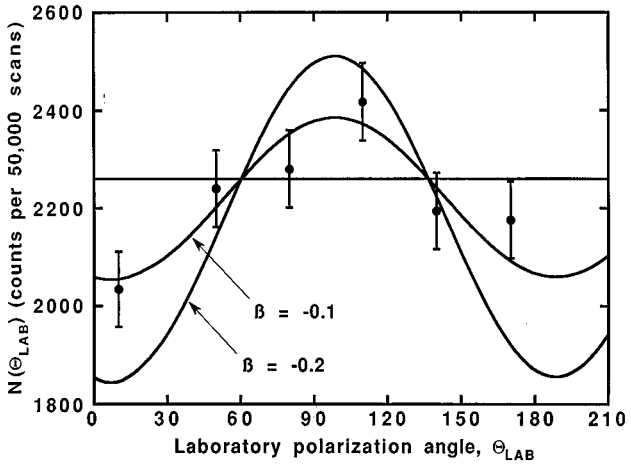

FIG. 11. The laboratory angular distribution of the Cl atom product from allyl chloride photodissociated at 193 nm with linearly polarized light. Θ_{LAB} is the angle of the laser electric vector with respect to detector axis. The data points show the signal integrated between 144–170 μs. Line fits show the predicted change in detected scattered signal intensity with laser polarization angle obtained, after transformation from the c.m. to the laboratory frame, with three trial anisotropy parameters; β=0.0, −0.1, and −0.2. The integrated signal also includes a minor contribution from the overlapping fast HCl elimination signal. The effect on the anisotropy parameter is probably minimal.

to determine the amount of the *gauche* conformer at both 20 °C and 90 °C which was 82%±9% and 78%±15%, respectively. From this data, they estimate an energy difference of 0.62 kcal/mol. The large error bars on the populations results in great uncertainty in the calculated energy difference. Using this *gauche/cis* energy difference of 0.62 kcal/mol, we can determine the relative change in conformer population upon heating the nozzle from 200 to 475 °C:[16]

$$\frac{(cis/gauche)_{475\,^\circ\mathrm{C}}}{(cis/gauche)_{200\,^\circ\mathrm{C}}}=\frac{0.87}{0.68}=1.3. \tag{2}$$

If only the *cis* conformer contributed to HCl elimination and only the *gauche* conformer contributed to C–Cl fission, then the relative change in the conformer population would predict an increase in the HCl/C–Cl branching ratio of 1.3. The experimentally observed change in the branching ratio, however, is significantly higher than the predicted change.

$$\frac{(\mathrm{HCl\ elimination/C{-}Cl\ fission})_{475\,^\circ\mathrm{C}}}{(\mathrm{HCl\ elimination/C{-}Cl\ fission})_{200\,^\circ\mathrm{C}}}=\frac{0.23}{0.12}=1.9. \tag{3}$$

Although the conformational energy difference may not be exact, an energy difference of 1.67 kcal/mol would be required to obtain a relative branching ratio change of 1.9. Thus, the increase in the HCl elimination/C–Cl fission branching ratio is not completely due to the change in conformer population.

We can also examine the competition between the two pathways for HCl elimination with C–Cl fission separately. The experimentally observed change in the HCl elimination channel leading to low recoil energies with C–Cl bond fission is determined from the relative probabilities used to fit the Cl^+ spectra in Figs. 7 and 9.

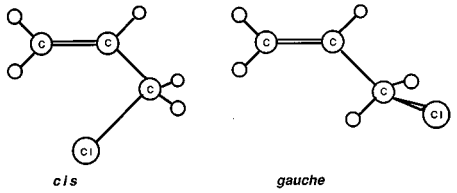

FIG. 12. The two conformers of allyl chloride; *cis* (left) and *gauche* (right).

$$\frac{\left(\dfrac{\text{slow HCl elimination}}{\text{C–Cl fission}}\right)_{475\,^\circ\mathrm{C}}}{\left(\dfrac{\text{slow HCl elimination}}{\text{C–Cl fission}}\right)_{200\,^\circ\mathrm{C}}}=\frac{\left(\dfrac{8.7\%}{71.5\%}\right)_{475\,^\circ\mathrm{C}}}{\left(\dfrac{3.0\%}{83.1\%}\right)_{200\,^\circ\mathrm{C}}}=3.4. \tag{4}$$

Similarly, the relative change in the HCl elimination producing fragments with high kinetic energy and C–Cl bond fission is determined.

$$\frac{(\text{fast HCl elimination/C–Cl fission})_{475\,^\circ\mathrm{C}}}{(\text{fast HCl elimination/C–Cl fission})_{200\,^\circ\mathrm{C}}}=\frac{(19.8\%/71.5\%)_{475\,^\circ\mathrm{C}}}{(13.9\%/83.1\%)_{200\,^\circ\mathrm{C}}}=1.7. \tag{5}$$

A marked increase in the slow HCl elimination channel occurs with a raise in the nozzle temperature and is too large to attribute to the change in the conformer populations. The increase in the fast HCl elimination channel, on the other hand, is less and may result from a conformation dependence. These results are further considered in Sec. IV.

D. Angular distribution of the C–Cl fission product

Figure 11 shows the integrated Cl fragment signal from C–Cl bond fission vs. Θ_{LAB}, the angle between the electric vector and the detector axis. The best fit is obtained by varying the anisotropy parameter β in this expression for the angular distribution of the fragments[17]

$$I(\theta_{\mathrm{c.m.}})=1/4[1+\beta P_2(\cos\ \theta_{\mathrm{c.m.}})] \tag{6}$$

in which $\theta_{\mathrm{c.m.}}$ is the angle between the electric vector and the recoiling fragment in the center-of-mass reference frame. Since the photofragment angular distribution is measured in the laboratory frame, fitting the data involves converting between the center-of-mass and laboratory frames using the measured molecular beam velocity and the $P(E_T)$ determined from the unpolarized data. The data in Fig. 11 shows the photofragment anisotropy for C–Cl bond fission to be slightly perpendicular with $\beta=-0.1$.[18] If we assume distortion of the molecule upon photoexcitation does not alter the C–Cl bond direction before dissociation and the transition dipole moment is parallel to the C═C bond, the predicted $\beta_{cis}=2P_2(\cos 63.1°)=-0.4$.[9(b)] The *gauche* conformer, however, is more complicated. The value predicted is $\beta_{gauche}=2P_2(\cos 127.4°)=0.11$.[9(b)] If the angle distorts by just 4°, the predicted β changes to −0.1. At a nozzle temperature of 220 °C, the molecular beam mixture is 79%

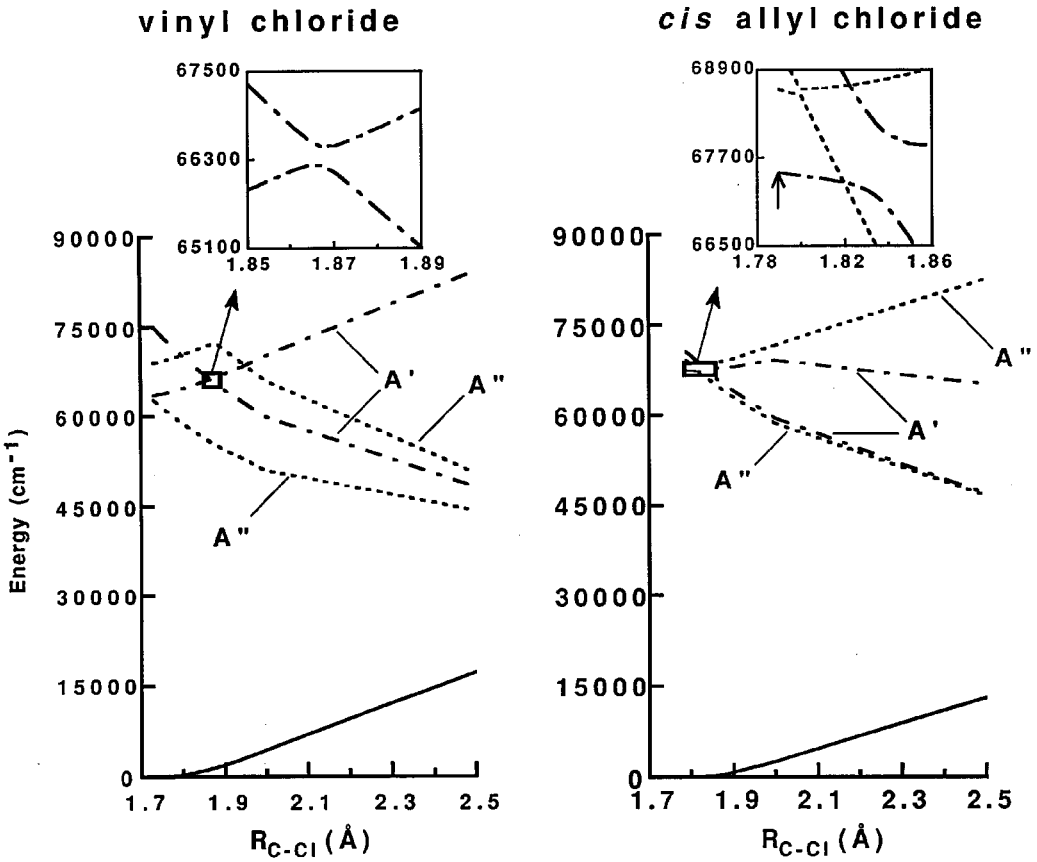

FIG. 13. Cuts through the calculated *ab initio* electronic surfaces at equilibrium C═C bond lengths, for vinyl chloride with R(C═C)=1.332 Å (left) and *cis*-allyl chloride with R(C═C)=1.316 Å (right). The four lowest singlet excited electronic states are shown. The two A' adiabatic states (– · –) are involved in the avoided electronic configuration crossing. The two A'' adiabatic states (– – –) are shown only because they fall in the same energy region; in planar symmetry, they do not interact with the A' states. The boxed-in portions are enlarged in the insets above to show the splitting between the adiabats at the avoided crossing. For the particular cut along the avoided crossing seam presented here, the splitting at the avoided crossing to C–Cl bond fission is 261 cm^{-1} for vinyl chloride and 982 cm^{-1} for *cis*-allyl chloride. For the *cis* conformer of allyl chloride, the inset also includes the Franck–Condon region (indicated by the arrow) and shows the potential is relatively flat.

gauche and 21% *cis* using the energy difference reported by Schei and Shen.[14] If only one conformer contributes to C–Cl fission, the expected β would correspond to the value predicted for that conformer. If, however, both conformers contribute equally to C–Cl fission, then the expected β would be a weighted average, $\beta=0.79(0.1)+0.21(-0.4)=0.0$. Since the predicted angular distribution for both conformers are similar and very sensitive to geometry change in the excited state, the angular distribution measurement is not sensitive enough to determine which conformer or weighted distribution of conformers undergoes C–Cl fission.

IV. DISCUSSION

The primary purpose of these experiments was to determine if the CH_2 spacer in allyl chloride as compared to vinyl chloride affects the probability of nonadiabatic recrossing of the barrier to C–Cl fission. The CH_2 spacer both further separates the C═C and the C–Cl chromophores and results in two molecular conformers, one of which does not retain a plane of symmetry. To illustrate why we expect the C–Cl bond fission pathway to be strongly influenced by nonadiabatic dynamics in these two systems, we first consider the excited state reaction coordinate for C–Cl fission in vinyl chloride. Umemoto *et al.*[5] characterized the pathway to C–Cl fission in vinyl chloride as a transition to the dissociative $n\sigma^*$ state which crosses the photoprepared $\pi\pi^*$ state in the C–Cl coordinate. In C_s symmetry, the out-of-plane π and $\pi^*_{C=C}$ orbitals are a'' and the in-plane n_{Cl} and σ^*_{C-Cl} orbitals are a'; therefore, both the $\pi\pi^*_{C=C}$ and the $n_{Cl}\sigma^*_{C-Cl}$ configurations are A' so that they mix and split forming a barrier along the lower adiabatic excited state potential energy surface. If the molecule traverses the barrier and accesses the region of the surface which is $n_{Cl}\sigma^*_{C-Cl}$ in character, C–Cl fission results. If, however, the splitting between the adiabatic electronic surfaces is small reflecting weak configurational mixing, a nonadiabatic transition to the upper adiabat can occur where the molecule retains its $\pi\pi^*$ configuration and turns back toward the Franck–Condon region instead of evolving to products along the lower surface. Thus, the magnitude of the splitting between the adiabats at the barrier reflects the probability that the barrier is traversed adiabatically.

The splitting is notably smaller for Woodward–Hoffmann forbidden reactions than for reactions where the

individual orbital symmetries are conserved.[2] Since the individual orbital symmetry changes from a'' to a' along the excited C–Cl reaction coordinate in vinyl chloride and *cis*-allyl chloride, C–Cl fission is Woodward–Hoffmann forbidden. Thus, we expect the splitting to be small and nonadiabatic barrier recrossing to reduce the rate constant for C–Cl fission. To argue qualitatively why we expect Woodward–Hoffmann forbidden reactions to have anomalously smaller splittings than reactions which conserve individual orbital symmetry, we calculate the configuration interaction matrix elements which mix and split the $\pi\pi^*$ and the $n\sigma^*$ configurations at the barrier to C–Cl fission. In a simple two-state system, the dominant electronic configuration contributing to the wave function on the reactant side of the barrier, Ψ_R, is $\{\cdots L(n_{\mathrm{Cl}})^2(\pi)^1(\pi^*)^1(\sigma^*_{\mathrm{C-Cl}})^0\}$ and for the wave function on the product side of the barrier, Ψ_P, is $\{\cdots L(n_{\mathrm{Cl}})^1(\pi)^2(\pi^*)^0(\sigma^*_{\mathrm{C-Cl}})^1\}$. If no orthogonality is assumed between the reactant and product molecular orbitals or between Ψ_R and Ψ_P, then the splitting between the two adiabatic surfaces at the barrier is[19]

$$\text{splitting} = \frac{2(\beta - \alpha S)}{(1-S^2)}, \tag{7}$$

where α is the energy at which the diabats cross, S is the overlap integral $\langle \Psi_R | \Psi_P \rangle / C$, and β is the interaction, resonance, or exchange energy $\langle \Psi_R | \mathscr{H} | \Psi_P \rangle / C$; C corrects for unnormalized wave functions. For Woodward–Hoffmann forbidden reactions, the product and reactant molecular orbitals are orthogonal by symmetry. As a result, the overlap integrals and all one-electron integrals that contribute to the resonance and exchange energy represented by β are zero so that only two-electron integrals mix and split the adiabats at the avoided crossing, resulting in a small splitting between the adiabats for this class of reactions.

Previous experiments in our lab have also demonstrated that increasing the distance between the orbitals involved in the avoided crossing increases the probability of nonadiabatically recrossing the barrier.[2,3] For example, the branching to C–Br bond fission upon $^1[n(\mathrm{O})\pi^*(\mathrm{C{=}O})]$ excitation decreased by an order of magnitude in bromopropionyl chloride compared to bromoacetyl chloride.[3] The extra CH_2 spacer between the $n_{\mathrm{O}}\pi^*_{\mathrm{C=O}}$ and the $n_{\mathrm{Br}}\sigma^*_{\mathrm{C-Br}}$ orbitals in bromopropionyl chloride reduces the electronic interaction matrix elements between the two configurations resulting in a smaller splitting between the adiabats at the barrier. Thus, C–Br fission is further suppressed by nonadiabatic barrier recrossing. Similarly, the branching to C–Cl fission might also decrease in allyl chloride compared to vinyl chloride.

Unlike vinyl chloride, allyl chloride exists as two conformers (Fig. 12). In the predominant *gauche* conformer, the Cl atom is out of the molecular plane breaking the plane of symmetry; therefore, C–Cl fission is no longer Woodward–Hoffmann forbidden, and we expect the splitting between the adiabats at the barrier to C–Cl fission to increase. As a result, the probability that the barrier to C–Cl fission is traversed adiabatically should be greater for *gauche*-allyl chloride than for vinyl chloride. The higher energy *cis* conformer, however, is planar so C–Cl fission is Woodward–Hoffmann forbidden. Thus, we expect C–Cl fission to be suppressed in the *cis* conformer, and the change in the HCl elimination/C–Cl fission branching ratio should follow the change in the fraction of the *cis* conformer. The data does show that the branching ratio increases with the raise in nozzle temperature, but the increase is stronger than that presented by the conformation dependence alone.

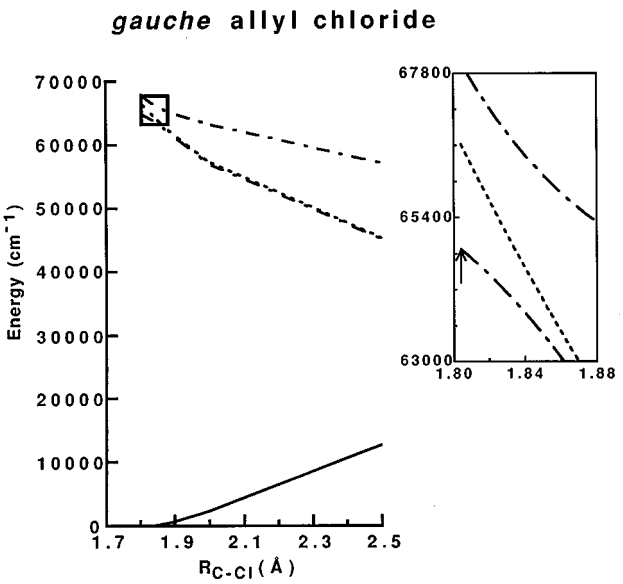

FIG. 14. Cuts through the calculated *ab initio* surfaces for *gauche*-allyl chloride at equilibrium C═C bond length, $R(\mathrm{C{=}C}) = 1.318$ Å. In the *gauche* conformer, only the three lowest singlet excited electronic states are shown (the next singlet excited state is above 70 000 cm^{-1}). Since the symmetry is broken, the $\pi\pi^*$ character, in principle, can mix into all three electronic states so that a two-state approximation may no longer be completely valid. By tracking the oscillator strengths (predominantly from $\pi\pi^*$ character) and the dominant electronic configurations of the excited state potential energy surfaces along the $R_{\mathrm{C-Cl}}$ coordinate, we can determine that primarily the first and third excited states (– · –) exhibit an avoided crossing around 1.84 Å. (The second excited state surface (- - -) does not participate significantly until 1.86 Å.) For the particular cut along the avoided crossing seam presented here, the splitting at the avoided crossing between the first and third adiabats is 2626 cm^{-1}. A larger splitting at the barrier between the two adiabats involved in the avoided electronic configuration crossing is seen here as compared to the *cis* conformer because C–Cl bond fission is now Woodward–Hoffmann allowed. The boxed-in portion is enlarged in the inset to the right to show the Franck–Condon region (indicated by the arrow). The inset has the same x/y aspect ratio as the inset for *cis*-allyl chloride in Fig. 13 in order to illustrate the different forces experienced in the Franck–Condon region for the two conformers. The repulsive forces in the C–Cl bond upon photoexcitation allow C–Cl fission to dominate in the *gauche* conformer.

We present GAUSSIAN 92 calculations in order to investigate the energetic splittings between the $^1A'$ excited potential energy surfaces at the avoided crossing for vinyl chloride and *cis*- and *gauche*-allyl chloride. Figure 13 shows cuts along the C–Cl stretch of the calculated *ab initio* electronic surfaces for vinyl and *cis*-allyl chloride. Although the four lowest singlet excited electronic surfaces are shown in Fig. 13, two are A'' so they do not interact with the A' surfaces in planar symmetry. The A' potential energy surface clearly evidences an avoided electronic curve crossing between the

$\pi\pi^*_{C=C}$ and $n_{Cl}\sigma^*_{C-Cl}$ states, forming the adiabatic reaction coordinate for C–Cl fission. Thus, the lower A' potential energy surface has a barrier along the forward and reverse reaction coordinate. As determined by the dominant electronic configuration in the GAUSSIAN 92 output, the electronic character changes from predominantly $\pi\pi^*_{C=C}$ to $n_{Cl}\sigma^*_{C-Cl}$ across the barrier in both systems. In vinyl chloride, the splitting between the adiabats at the barrier to C–Cl fission is very small which supports the model that nonadiabatic barrier recrossing can reduce the rate constant for C–Cl fission and allow HCl elimination to compete. The branching ratio measured by Mo *et al.*[4] for vinyl chloride, HCl:C–Cl $=1.0:1.1$, shows the two pathways are competing. The splitting at the barrier calculated for vinyl chloride is surprisingly smaller than for *cis*-allyl chloride even though a CH_2 spacer is inserted between the C=C and C–Cl chromophores in the latter. This may result from an increase in the overlap densities between the chromophores since in the *cis* conformer, the Cl atom eclipses the double bond. As expected for the *gauche* conformer in which C–Cl fission is no longer Woodward–Hoffmann forbidden, the splitting is much larger (see Fig. 14), and C–Cl fission can proceed adiabatically and dominate HCl elimination. Figure 14 also shows that in the Franck–Condon region for the *gauche* conformer, the forces are repulsive in the C–Cl bond along the C–Cl bond fission reaction coordinate. In the *cis* conformer, the contour is relatively flat in the Franck–Condon region along the C–Cl bond fission pathway. The repulsive forces in the Franck–Condon region for the *gauche* conformer should allow C–Cl fission to occur more readily. The experiments confirm that the branching to C–Cl fission has increased; the measured branching ratio for allyl chloride is $(HCl:C-Cl)_{200\,°C} = 0.12:1.0$. Further calculations are planned which will consider torsion about the double bond and C=C stretching since these motions are important upon excitation.[20]

Our laboratory has also measured the emission spectra at 199 nm for vinyl chloride and allyl chloride in order to elucidate the electronic character of the excited states in the Franck–Condon region.[20] The emission spectrum for vinyl chloride evidences the dominant $\pi\pi^*$ character of the initial excitation by the strong emission to the C=C stretching and twisting modes. The *ab initio* calculations presented in that work and augmented in this paper agree with the emission spectrum; they show the electronic character of the bright $^1A'$ potential energy surface in vinyl chloride is $\pi\pi^*$ in the Franck–Condon region (Fig. 15). Upon electronic excitation of allyl chloride, however, enhanced emission into the C–Cl stretch eigenstates appear (although the C=C stretch still dominates), revealing an admixture of $\pi^*_{C=C}$ and σ^*_{C-Cl} character in the Franck–Condon region. The emission spectrum for allyl chloride reflects the initial motion in the predominant *gauche* conformer of allyl chloride upon photoexcitation. The calculations also show an increased contribution of σ^*_{C-Cl} character to the optically bright state (Fig. 16, bottom). Similar to vinyl chloride, the calculations for *cis*-allyl chloride reflect the pure $\pi\pi^*$ character in the Franck–Condon region (Fig. 16, top). The broken symmetry in the *gauche* conformer permits extensive coupling between the $\pi\pi^*$ and

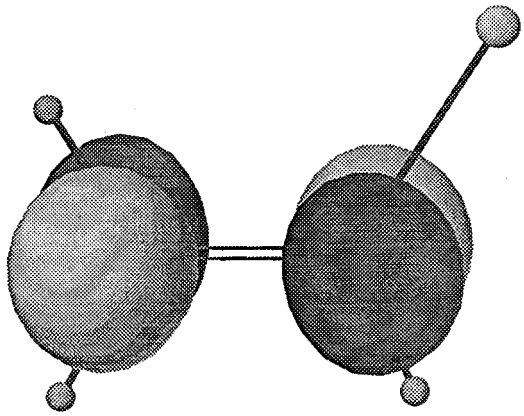

FIG. 15. The excited state molecular orbital for vinyl chloride from the bright state in the Franck–Condon region. The orbital shows essentially pure $\pi^*_{C=C}$ character. Figure reproduced with permission of the authors from Ref. 20.

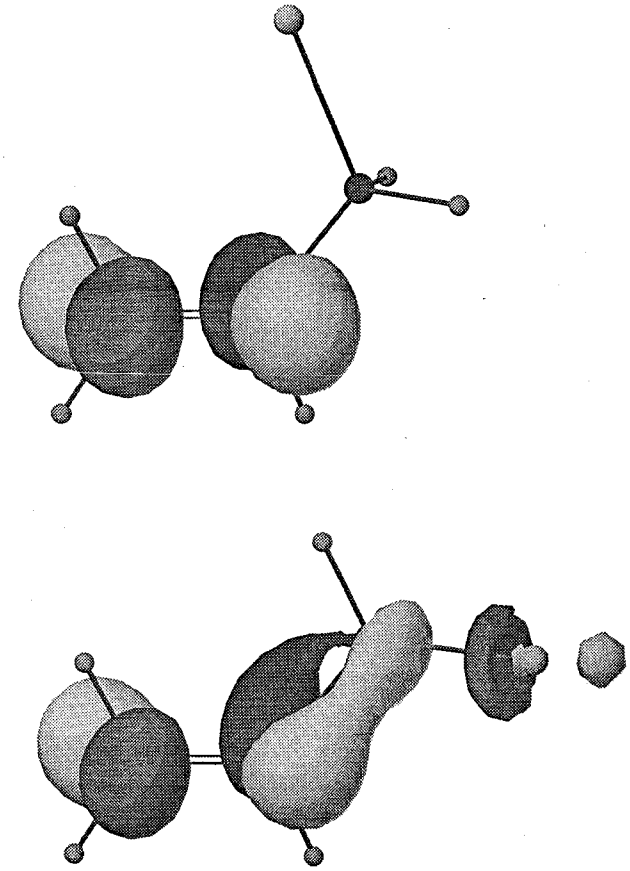

FIG. 16. The top frame shows the excited state molecular orbital for *cis* allyl chloride from the bright state in the Franck–Condon region. The orbital illustrates the essentially pure $\pi^*_{C=C}$ character. The bottom frame shows the dominant excited state molecular orbital for *gauche*-allyl chloride from the bright state in the Franck–Condon region. The orbital has an admixture of $\pi^*_{C=C}$ and σ^*_{C-Cl} character. Figures reproduced with permission of the authors from Ref. 20.

$n\sigma^*$ electronic configurations and results in repulsive forces along the C–Cl reaction coordinate in the Franck–Condon region, reflected also in the slope of the potential in Fig. 14, which allows C–Cl fission to dominate HCl elimination.

We now discuss likely explanations for the two observed pathways for HCl elimination in allyl chloride. In vinyl chloride, HCl elimination is believed to occur following internal conversion to the ground electronic state in which two different mechanisms were elucidated: a three-center, $\alpha\alpha$ elimination of HCl to produce vinylidene and a four-center, $\alpha\beta$ elimination of HCl to produce acetylene with a product ratio of $\alpha\alpha$:$\alpha\beta$=3:1.[21] The H atom transfer in vinylidene has a low barrier and occurs fast on the timescale of the reaction. The exit barrier for the four-center elimination is 52.6 kcal/mol and the exit barrier for the three-center elimination and subsequent H atom migration to produce acetylene is 44.1 kcal/mol.[9] Since the three-center elimination dominates over the four-center elimination and both channels have similar exit barriers, the HCl elimination pathway in vinyl chloride was fit using only one broad translational energy distribution.

In allyl chloride, however, two different translational energy distributions must be used to fit the data. The HCl elimination could occur from dynamics either on the ground state potential energy surface after internal conversion or on an excited state potential energy surface. Several different mechanisms for the HCl elimination are possible:[22]

$$H_2C{=}CHCH_2Cl + 193\ \text{nm} \rightarrow H_2C{=}C{=}CH_2 + HCl, \quad E_{\text{avail}} = 124\ \text{kcal/mol}, \tag{8}$$

$$H_2C{=}CHCH_2Cl + 193\ \text{nm} \rightarrow H_2C{=}C\ddot{C}H + HCl, \quad E_{\text{avail}} = 95\ \text{kcal/mol}, \tag{9}$$

$$H_2C{=}CHCH_2Cl + 193\ \text{nm} \rightarrow H\dot{C}{=}CH\dot{C}H_2 + HCl, \quad E_{\text{avail}} = 73\ \text{kcal/mol}. \tag{10}$$

Another possibility is hydrogen atom migration to produce $H_3C\ddot{C}CH_2Cl$ or $H_2\ddot{C}CHCH_2Cl$ which subsequently undergoes HCl elimination. The present experiment does not provide enough information to definitively identify the mechanism involved in both HCl elimination pathways. However, the very high energies of 76 kcal/mol detected in product recoil for the HCl elimination channel in the upper frame of Fig. 5 suggest this channel is most likely due to the mechanism presented in reaction (8). The low energy signal probably results from reaction (9) or (10). More information is needed about the exit barriers for these reactions in order to form any definite conclusions.

The temperature dependence of the HCl elimination channels provide a further clue as to their mechanism. As shown in Sec. III C, the branching to the HCl elimination producing fragments with low kinetic energy increases more than the channel producing the fast HCl fragments with a raise in nozzle temperature. When we attempted to attribute all of the HCl elimination to the *cis* conformer and all of the C–Cl fission to the *gauche* conformer, the observed increase in the HCl/C–Cl branching ratio upon heating the nozzle from 200 °C to 475 °C was higher than the relative change in the *cis/gauche* conformer population. Instead, let us now assume that the fast HCl channel occurs predominantly from the *cis* conformer whereas the slow HCl channel and C–Cl fission occur predominantly from the *gauche* conformer. Then, the change in the relative branching between HCl(fast)/[HCl(slow)+C–Cl] should follow the change in the conformer population upon heating the nozzle.

$$\frac{(\text{fast HCl elimination}/(\text{slow HCl elimination}+\text{C–Cl fission}))_{475\,^\circ\text{C}}}{(\text{fast HCl elimination}/(\text{slow HCl elimination}+\text{C–Cl fission}))_{200\,^\circ\text{C}}} = \frac{(19.8\%/(8.7\%+71.5\%))_{475\,^\circ\text{C}}}{(13.9\%/(3.0\%+83.1\%))_{200\,^\circ\text{C}}} = 1.5.$$

This result is similar to the relative change in the conformer population in heating the nozzle from 200 to 475 °C, which was previously shown to be 1.3.

We present a plausible explanation for the large increase in the slow HCl elimination channel with a raise in nozzle temperature. Going from a 200 °C to 475 °C nozzle expansion results in increased initial excitation of low energy vibrational motion. Umemoto *et al.*[5] claim that out-of-plane motion in vinyl chloride increases the coupling between the $\pi\pi^*$ and the $\pi\sigma^*$ state leading to efficient internal conversion to the $\pi\sigma^*$ state which they propose opens up the doorway to the ground state. In allyl chloride, the increased bending motion at the higher temperature increases the coupling with the predominantly $\pi\sigma^*$ state which may also serve as the intermediate state for internal conversion to the ground state.

In the final stages of preparation of this work, we learned that Lee *et al.*[7] have also recently investigated the photodissociation of allyl chloride at 193 nm. They report the major channel is C–Cl fission, but they only report one channel for HCl elimination with an average translational energy of 9 kcal/mol accounting for 5% of the total product yield.

ACKNOWLEDGMENTS

This work was supported by the National Science Foundation under Grant No. CHE-9307500. T.L.M. was supported by a Department of Education GAANN fellowship.

[1] R. B. Woodward and R. Hoffmann, *The Conservation of Orbital Symmetry* (Verlag-Chemie, Weinheim, 1970); S. S. Shaik, J. Am. Chem. Soc. **103**, 3692 (1981).
[2] G. C. G. Waschewsky, P. W. Kash, T. L. Myers, D. C. Kitchen, and L. J. Butler, J. Chem. Soc. Faraday. Trans. **90**, 1581 (1994).
[3] P. W. Kash, G. C. G. Waschewsky, L. J. Butler, and M. M. Francl, J. Chem. Phys. **99**, 4479 (1993).

[4] Y. Mo, K. Tonokura, Y. Matsumi, M. Kawasaki, T. Sato, T. Arikawa, P. T. A. Reilly, Y. Xie, Y. A. Yang, Y. Huang, and R. J. Gordon, J. Chem. Phys. **97**, 4815 (1992).
[5] M. Umemoto, K. Seki, H. Shinohara, U. Nagashima, N. Nishi, M. Kinoshita, and R. Shimada, J. Chem. Phys. **83**, 1657 (1985).
[6] C. W. Worrell, J. Electron. Spectrosc. **3**, 359 (1974).
[7] Private communication of recent results by Y. R. Lee, F. T. Chen, and S. M. Lin, submitted for publication in J. Chem. Phys.
[8] T. S. Sears and D. H. Volman, J. Photochem. **26**, 85 (1984).
[9] (a) The equilibrium geometry for vinyl chloride is taken from J. F. Riehl and K. Morokuma, J. Chem. Phys. **100**, 8976 (1994); (b) The equilibrium geometries for *cis*- and *gauche*-allyl chloride are taken from J. R. Durig, D. T. Durig, M. R. Jalilian, M. Zhen, and T. S. Little, J. Mol. Struc. **194**, 259 (1989). The values calculated with the 6-31G* basis set were used.
[10] GAUSSIAN 92, Revision C, M. J. Frisch, G. W. Trucks, M. Head-Gordon, P. M. W. Gill, M. W. Wong, J. B. Foresman, B. G. Johnson, H. B. Schlegel, M. A. Robb, E. S. Replogle, R. Gomperts, J. L. Andres, K. Raghavachari, J. S. Binkley, C. Gonzalez, R. L. Martin, D. J. Fox, D. J. Defrees, J. Baker, J. J. P. Stewart, and J. A. Pople (Gaussian, Inc., Pittsburgh, PA, 1992).
[11] The bond dissociation energies were taken from A. Streitwieser, Jr., and C. H. Heathcock, *Introduction to Organic Chemistry* (Macmillan, New York, 1985), 3rd ed.
[12] We estimated the ionization cross sections using the empirical relationship obtained in R. E. Center and A. Mandl, J. Chem. Phys. **57**, 4104 (1972), $\sigma_{\text{ion}}(10^{-16}\ \text{Å}^2)=36(\alpha^{1/2})-18$. The atomic polarizability of 2.18 Å^3 for Cl is given in T. M. Miller and B. Bederson, Adv. At. Mol. Phys. **13**, 1 (1977), and the molecular polarizability of 2.60 Å^3 for HCl is given in N. J. Bridge and A. D. Buckingham, Proc. R. Soc. London, Ser. A **295**, 334 (1966).
[13] R. S. Ruoff, T. D. Klots, T. Emilsson, and H. S. Gutowsky, J. Chem. Phys. **93**, 1 (1990).
[14] S. H. Schei and Q. Shen, J. Mol. Struc. **128**, 161 (1985).
[15] A. J. Barnes, S. Holroyd, W. O. George, J. E. Goodfield, and W. F. Maddams, Spectrochim. Acta **38A**, 1245 (1982).
[16] Although the *gauche* populations of 82% and 78% at 20 °C and 90 °C respectively would give an energy difference of 0.75 kcal/mol (and a nonzero entropy change), the authors from Ref. 14 report an enthalpy difference of 0.62 kcal/mol. The value of 0.62 kcal/mol was probably derived from the populations before they were rounded to two significant figures (for example, percentages of 81.6 and 78.3 give 0.62 kcal/mol); thus we retain the 0.62 kcal/mol value here. If the entropy change is considered to be negligible, then the calculated energy difference becomes approximately 0.43 kcal/mol. If we recalculate the relative change in conformer population upon heating the nozzle from 200 °C to 475 °C with an energy difference of 0.44 ± 0.03 kcal/mol, the ratio changes only slightly to 1.2.
[17] R. N. Zare, Mol. Photochem. **4**, 1 (1972).
[18] The measured angular distribution may depend on the nozzle temperature if both conformers contribute to C–Cl fission due to the change in the conformer population. Results by Y. R. Lee, F. T. Chen, and S. M. Lin, submitted to J. Chem. Phys. measure $\beta=0.2$ at 170 °C; this result suggests C–Cl fission occurs predominantly from the *gauche* conformer.
[19] For a more detailed explanation of this argument see Ref. 2. Also, see D. M. Silver, J. Am. Chem. Soc. **96**, 5959 (1974).
[20] P. W. Browning, D. C. Kitchen, M. F. Arendt, and L. J. Butler, J. Phys. Chem. (in press).
[21] Y. Huang, Y. A. Yang, G. X. He, and R. J. Gordon, J. Chem. Phys. **99**, 2752 (1993).
[22] The heats of formation for reaction (8) were taken from R. C. Weast, *Handbook of Chemistry and Physics* (Chemical Rubber, Boca Raton, FL, 1983), Vol. 64. Reactions (9) and (10) were estimated from the bond strengths in D. F. McMillen and D. M. Golden, Annu. Rev. Phys. Chem. **33**, 493 (1982) and exclude any resonance stabilization energy.